EURASIP Journal on Wireless Communications and Networking
a SpringerOpen Journal

RESEARCH Open Access

M-ary energy detection of a Gaussian FSK UWB system

Song Cui* and Fuqin Xiong

Abstract

The energy detection M-ary Gaussian frequency-shift keying (FSK) system is proposed in this paper. The system performance is analyzed in additive white Gaussian noise channels, multipath channels, and in the presence of synchronization errors. The numerical results show that the M-ary modulation achieves the higher data rate than the binary modulation. However, it also results in performance degradation.

1 Introduction

Energy detection (ED) is a popular technology in ultra-wideband (UWB) communication systems. When compared to Rake receivers, ED has as many advantages, such as simple receiver structure [1,2], robustness to synchronization errors, and no channel estimation requirement. The popular ED schemes include on-off keying (OOK) and pulse position modulation (PPM) [3]. In our previous publication [4], a new ED scheme based on using different-order derivatives of the Gaussian pulse was proposed. This new scheme is called Gaussian frequency-shift keying (GFSK) energy detection UWB. It was proved that this new scheme has better bit error rate (BER) performance than an energy detection PPM UWB system in multipath channels and in the presence of synchronization errors.

In [4], the energy detection Gaussian FSK system is based on binary modulation so we extend the research into M-ary modulation in this paper.

Although there exist some M-ary UWB methods, our method is different to these methods. In [5], the M-ary modulation is achieved by using the orthogonality of modified Hermite polynomials $h_n(t) = (-1)^n e^{\frac{t^2}{4}} \frac{d^n}{dt^n}(e^{\frac{-t^2}{2}})$. Where n is the order of the polynomials and $n = 0, 1, |\ldots,$ and $-\infty < t < \infty$. In [6], the waveform is obtained from the Battle-Lemarie wavelet $\psi(t) = \sqrt{2}\sum_l \sum_k g_l c_k \beta_n(2t - l - k)$, where g_l and c_k are coefficients, and $\beta_n(t)$ is a B-spline function of order n. In [7], the author uses the pulsed sinusoidal waveform as carrier to realize the M-ary FSK modulation. In this paper, we will construct the M-ary FSK waveforms using different order derivatives of the Gaussian pulse. The spectra of these different-order derivatives of the Gaussian pulses are separated entirely in frequency domain so the orthogonality is achieved. Our M-ary FSK system still transmits baseband pulses without inducing carrier modulation. UWB is carrier-less system, so our method conforms to UWB regulation. At the receiver, the demodulation can be achieved by using filters with different passband frequencies to separate the pulses directly. This makes it very simple and easy to implement the demodulation procedure.

The structure of this paper is as follows: Section 2 introduces the system models. Section 3 evaluates system performance in additive white Gaussian noise (AWGN) channels. Section 4 evaluates system performance in multipath channels. The effect of synchronization errors on system performance is analyzed in Section 5. In Section 6, the numerical results are analyzed. Section 7 is the conclusion.

2 System models

Before we develop the M-ary Gaussian FSK system, we will briefly summarize the system model of binary modulation in [4]. The Fourier transform X_f and center frequency f_c of the kth-order derivative are given by

$$X_f \propto f^k \exp(-\pi f^2 \alpha^2/2) \tag{1}$$

$$f_c = \sqrt{k}/(\alpha\sqrt{\pi}) \tag{2}$$

*Correspondence: s.cui99@csuohio.edu
Department of Electrical and Computer Engineering, Cleveland State University, Cleveland, OH 44115-2214, USA

where k is the order of the derivative and f is the frequency. The pulse shape factor is denoted by α. When the value of α is fixed and the value of k is changed, we obtain spectral curves for different-order derivatives of the Gaussian pulse. Those curves have similar shapes and bandwidths but their center frequencies are different. If the values of k and α are appropriately chosen, it is always possible to separate the spectra of the two pulses. Exploiting the spectral characteristics of the pulses, the transmitter of the Gaussian FSK system is as follows.

$$s(t)_{\mathrm{GFSK}} = \sum_j \sqrt{E_p}(b_j p_1(t - jT_f) + (1 - b_j)p_2(t - jT_f)) \tag{3}$$

where $p_1(t)$ and $p_2(t)$ denote the pulses of different-order derivatives with normalized energy and E_p is the signal energy. The jth transmitted bit is denoted by b_j. The frame period is denoted by T_f. The modulation is carried out as follows: when bit 1 is transmitted, the value of b_j and $1-b_j$ are 1 and 0, respectively, so $p_1(t)$ is transmitted. Similarly, the transmitted pulse for bit 0 is $p_2(t)$. The above transmitter considers a single user only, and a bit is transmitted once. The receiver includes two branches, and each branch is a conventional energy detection receiver. The only difference between the two branches is the passband frequency ranges of filters. The filter in the first branch is designed to pass the signal energy of $p_1(t)$ and reject that of $p_2(t)$, and the filter in the second branch passes the signal energy of $p_2(t)$ and rejects that of $p_1(t)$. Finally, the captured energies of two branches are subtracted to generate a decision variable and then this variable is compared with decision threshold to determine the transmitted bit. If the decision variable is greater than decision threshold, the transmitted bit is 1, otherwise it is 0. The abovementioned is the brief description of the transmitter and receiver of the energy detection GFSK UWB system in [4].

In this paper, we will develop the M-ary system as follows: The transmitter of the M-ary system is

$$s(t) = \sum_j \sqrt{E_p} p^{(M_j)}(t - jT_f) \tag{4}$$

where $p^{(M_j)}$ denotes the transmitted pulse for the jth symbol and $p^{(M_j)}$ is the derivative of the Gaussian pulse. The order of the derivative is given by the value of M_j. We will use an example to show how to assign a value for M_j according to the transmitted data. For example, we use a 4-ary system in the followed analysis and every two bits are encoded in to a symbol using Gray code. Figure 1 shows the spectral curves of the pulses for the different bit groups. The four curves have the same bandwidth and different center frequencies. They are orthogonal so they can be separated at the receiver. The bit groups of 00, 01, 11, and 10 are corresponding to the spectral curves from the left to right in Figure 1. The orders of the derivatives of these four curves are 52, 110, 190, and 290, respectively. To make sure that the spectra of the selected curves meet the Federal Communications Commission (FCC) emission mask, we add the emission mask. For convenience in observation, we convert the linear scale of Figure 1 into the logarithmic scale of Figure 2. In Figure 2, it is straightforward to see that all of the curves meet the emission requirement set by the FCC. The receiver structure is shown in Figure 3. The receiver has four branches. The only difference of these branches is the passbands of the filters. The filters in each branch can capture the energy of only one signal and suppress the energy of the other signals. In Figure 3, branches 1, 2, 3, and 4 capture the energy of the pulses with orders of 52, 110, 190, and 290, respectively. The shape factor is $\alpha = 1 \times 10^{-9}$, and the width of the pulses is 2.4×10^{-9}. In other words, these four branches capture the signal energies corresponding to bit groups 00, 01, 11, and 10, respectively. Finally, the decision is based on comparing the captured energies of the four branches. The branch with the largest energy is chosen.

3 SER performance in AWGN channels

3.1 SER performance of GFSK in AWGN channels

Assuming symbols 0, 1, 2, and 3 are transmitted with equal probability, the symbol error rate (SER) is calculated as

$$P_e = \frac{1}{4}p_{e_0} + \frac{1}{4}p_{e_1} + \frac{1}{4}p_{e_2} + \frac{1}{4}p_{e_3} \tag{5}$$

where p_{e_0}, p_{e_1}, p_{e_2}, and p_{e_3} denote the SER when symbols 0, 1, 2, and 3 are transmitted, respectively. We will define how a detection error occurs as follows. When a symbol is transmitted, the captured signal energy in the branch corresponding to that symbol is not the largest, we can claim a detection error occurs. For example, when symbol 0 is transmitted, the error detection occurs if any of the captured signal energies from branch 1, 2, and 3 is greater than that of branch 0. When symbol 0 is transmitted, the SER can be expressed as

$$P_{e0} = 1 - P_{c0} \tag{6}$$

where P_{c0} denotes the probability of the successful detection when symbol 0 is transmitted. When the captured energy of branch 0 is greater than that of all the other branches, the signal is successfully detected. So we have

$$P_{c_0} = P_{c_{01}} P_{c_{02}} P_{c_{03}} = (1 - P_{e_{01}})(1 - P_{e_{02}})(1 - P_{e_{03}}) \tag{7}$$

where $P_{c_{01}}$, $P_{c_{02}}$, and $P_{c_{03}}$ denote the probability that the captured energy of branch 0 is greater than those of

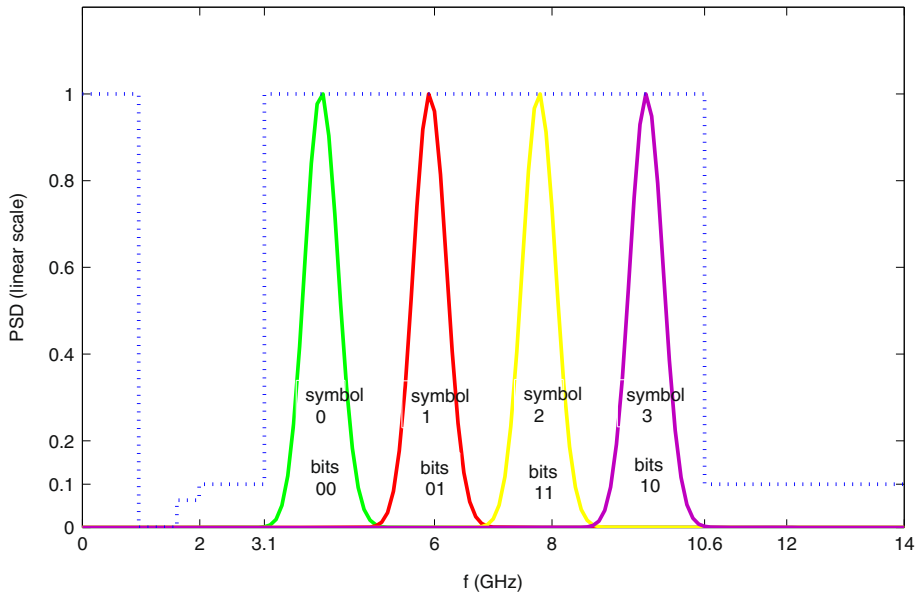

Figure 1 **PSD of pulses versus FCC emission mask (logarithmic scale).**

branches 1, 2, and 3, respectively. And $P_{e_{01}}$, $P_{e_{02}}$, and $P_{e_{03}}$ denote the probability that the captured energy of branch 0 is less than those of branches 1, 2, and 3, respectively. Substituting (7) into (6), we have

$$P_{e_0} = 1 - (1 - P_{e_{01}})(1 - P_{e_{02}})(1 - P_{e_{03}}) \tag{8}$$

The calculation of P_{e_0} is converted to calculate $P_{e_{01}}$, $P_{e_{02}}$, and $P_{e_{03}}$. In Figure 3, $Z_{j,0}$, $Z_{j,1}$, $Z_{j,2}$, and $Z_{j,3}$ are chi-square variables with approximately a degree $2TW$ [8], where T denotes the integration time and W denotes the bandwidth of the filtered signals. Gaussian approximation has been a popular method to simplify the derivation of BER equation in energy detection UWB systems. When UWB signals pass through the channel, the long channel delay leads to a very large $2TW$ value and Gaussian approximation can achieve accurate result. The application of Gaussian approximation in energy detection UWB systems can be seen in [2-4,9-14]. The

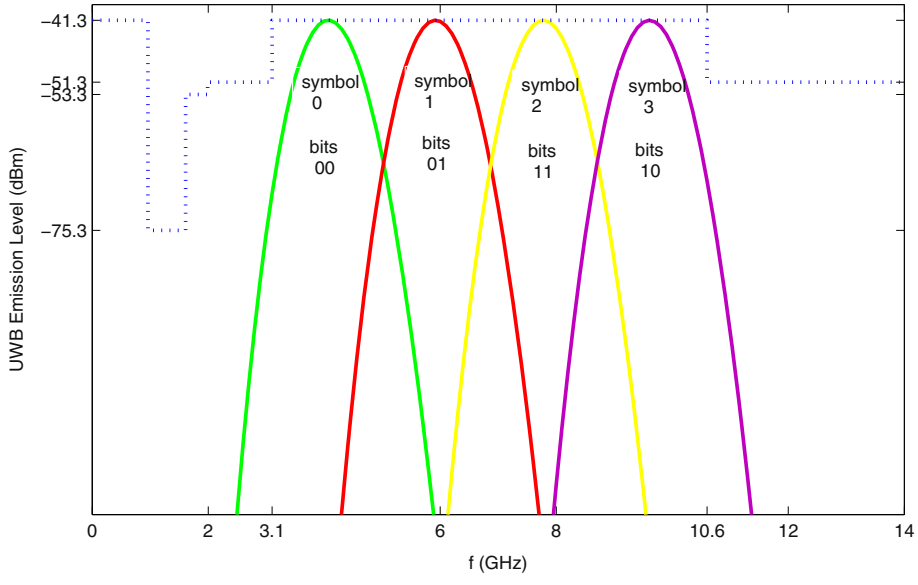

Figure 2 **PSD of pulses versus FCC emission mask (linear scale).**

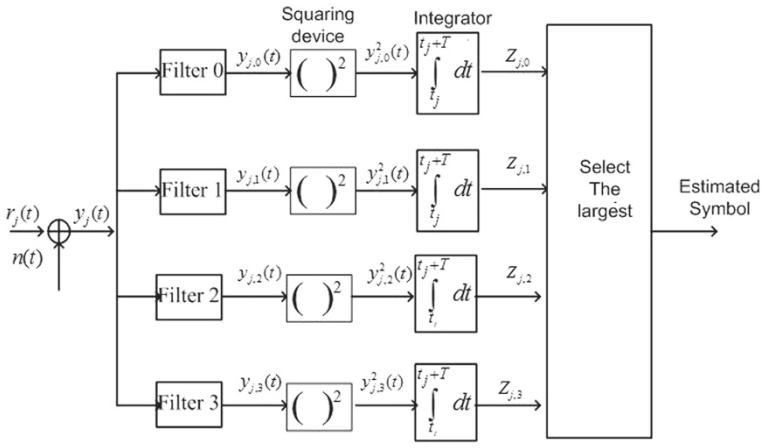

Figure 3 Receiver of a GFSK UWB system.

chi-square variable can be approximated as Gaussian variables [4,15].

$$\mu = N_0 TW + E \tag{9}$$

$$\sigma^2 = N_0^2 TW + 2N_0 E \tag{10}$$

where μ and σ^2 are the mean value and variance, respectively. The double-sided power spectral density of AWGN is $N_0/2$. And T denotes the integration time, W denotes the bandwidth of filter. The signal energy which passes through the filter is denoted by E. If the filter rejects all of the signal energy, then $E = 0$. In Figure 3, when symbol 0 is transmitted, the signal energy passes through filter 0 and is rejected by the other filters. The probability density function (pdf) of $Z_{j,0}$ is $Z_{j,0} \sim N(N_0 TW + E_s, N_0^2 TW + 2N_0 E_s)$, where E_s denotes the symbol energy and j denotes the jth transmitted symbol. When symbol 0 is transmitted, $Z_{j,1}$, $Z_{j,2}$, and $Z_{j,3}$ have the same probability density function $Z_{j,1} = Z_{j,2} = Z_{j,3} \sim N(N_0 TW, N_0^2 TW)$. Firstly, we calculate $P_{e_{01}}$ as follow.

$$P_{e_{01}} = P(Z_{j,0} < Z_{j,1}) \tag{11}$$

It can be converted to calculate $P_{e_{01}} = P(Z_{j,0} - Z_{j,1} < 0)$. The probability density function of $Z_{j,0} - Z_{j,1}$ is $Z_{j,0} - Z_{j,1} \sim N(E_s, 2N_0^2 TW + 2N_0 E_s)$. We can achieve

$$\begin{aligned} P_{e_{01}} &= \int_{-\infty}^{0} \frac{1}{\sqrt{2\pi}\sqrt{2N_0^2 TW + 2N_0 E_s}} e^{-\frac{(x-E_s)^2}{2(2N_0^2 TW + 2N_0 E_s)}} dx \\ &= Q\left(\frac{E_s}{\sqrt{2N_0^2 TW + 2N_0 E_s}}\right) \end{aligned} \tag{12}$$

where $Q(\cdot)$ is the complementary error function. Using the same method, we achieve

$$P_{e_{02}} = P_{e_{03}} = Q\left(\frac{E_s}{\sqrt{2N_0^2 TW + 2N_0 E_s}}\right) \tag{13}$$

Substituting (12) and (13) into (8), we achieve

$$P_{e_0} = 1 - \left(1 - Q\left(\frac{E_s}{\sqrt{2N_0^2 TW + 2N_0 E_s}}\right)\right)^3 \tag{14}$$

Similarly, we can achieve

$$P_{e_1} = P_{e_2} = P_{e_3} = 1 - \left(1 - Q\left(\frac{E_s}{\sqrt{2N_0^2 TW + 2N_0 E_s}}\right)\right)^3 \tag{15}$$

Substituting (14) and (15) into (5), we achieve the SER in AWGN channels

$$P_e = 1 - \left(1 - Q\left(\frac{E_s}{\sqrt{2N_0^2 TW + 2N_0 E_s}}\right)\right)^3 \tag{16}$$

The above equation can be extended to the M-ary modulation as

$$P_e = 1 - \left(1 - Q\left(\frac{E_s}{\sqrt{2N_0^2 TW + 2N_0 E_s}}\right)\right)^{M-1} \tag{17}$$

If $M = 2$, Equation 17 will be reduced to

$$P_e = Q\left(\frac{E_s}{\sqrt{2N_0^2 TW + 2N_0 E_s}}\right) \tag{18}$$

Equation 18 is the SER of binary GFSK in AWGN channels, and it is the same as that in [4].

4 SER performance in multipath channels

In this section, the SER performances of PPM and GFSK in multipath channels are researched. The channel model of the IEEE 802.15.4a standard [16] is used in this paper. After the signal travels through a multipath channel, it is convolved with the channel impulse response. The received signal becomes

$$r(t) = s(t) \otimes h(t) + n(t) \tag{19}$$

where $h(t)$ denotes the channel impulse response and $n(t)$ is AWGN. The symbol $\otimes$ denotes the convolution operation. The IEEE 802.15.4a model is an extension of the Saleh-Valenzeula (S-V) model. The channel impulse response is

$$h(t) = \sum_{l=0}^{L} \sum_{k=0}^{K} \alpha_{k,l} \exp(j\phi_{k,l}) \delta(t - T_l - \tau_{k,l}) \tag{20}$$

where $\delta(t)$ is the Dirac delta function, and $\alpha_{k,l}$ is the tap weight of the kth component in the lth cluster. The delay of the lth cluster is denoted by T_l and $\tau_{k,l}$ is the delay of the kth multipath component relative to T_l. The phase $\phi_{k,l}$ is uniformly distributed in the range $[0, 2\pi]$.

Figure 4 is the frame structure of M-ary GFSK in multipath channels. The integration interval T_0 is less or equal to the maximum channel spread of GFSK. The synchronization is assumed to be perfect in analysis. The guard interval is T_g, and the frame period is set to $T_f = T_0 + T_g = D$. This will achieve the maximum data rate and prevent inter-frame interference (IFI) simultaneously. This frame structure is applied to all symbols. Assuming symbol 0 is transmitted, the pdfs of $Z_{j,0}$ is $Z_{j,0} \sim N(N_0TW + \lambda E_s, N_0^2TW + 2N_0\lambda E_s)$. And $Z_{j,1}$, $Z_{j,2}$, and $Z_{j,3}$ have the same pdfs $Z_{j,1} = Z_{j,2} = Z_{j,3} \sim N(N_0TW, N_0^2TW)$. Following the same method in Section 3, we achieve the SER in multipath channels

$$P_e = 1 - \left(1 - Q\left(\frac{\lambda E_s}{\sqrt{2N_0^2TW + 2N_0\lambda E_s}}\right)\right)^3 \tag{21}$$

where λ denotes the ratio of the captured energy of a symbol. The value of λ is related to the integration interval. The longer integration interval will capture more energy. Due to the randomness of the channel parameters, there is no direct equation to calculate the value of λ [4]. We can follow the method in [4] to achieve the value of λ. The SER value should be averaged over many channel realizations. We will explain these more detailed in numerical analysis of Section 6. The above equation can be extended to the M-ary modulation as follows:

$$P_e = 1 - \left(1 - Q\left(\frac{\lambda E_s}{\sqrt{2N_0^2TW + 2N_0\lambda E_s}}\right)\right)^{M-1} \tag{22}$$

If binary modulation is used, $M = 2$, and Equation 22 is reduced to

$$P_e = Q\left(\frac{\lambda E_s}{\sqrt{2N_0^2TW + 2N_0\lambda E_s}}\right) \tag{23}$$

Equation 23 is SER of binary GFSK in multipath channels, and it is the same as in [4].

5 Performance analysis in the presence of synchronization errors

Figure 5 depicts the GFSK frame structures when synchronization errors ε occur. Assuming that coarse synchronization has been achieved, the SER performance of GFSK are analyzed in the range $\varepsilon \in [0, D/2]$. To prevent IFI, the frame length is set to $T_f = 2D + T_g$, where the guard interval T_g equals to $D/2$, the maximum synchronization error used in this paper. Assuming symbol 0 is transmitted, the pdfs of $Z_{j,0}$ is $Z_{j,0} \sim N(N_0TW +$

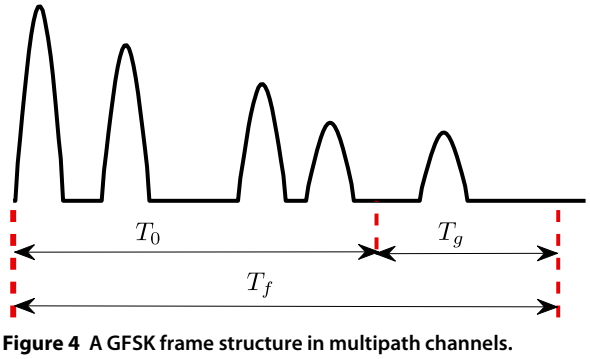

Figure 4 A GFSK frame structure in multipath channels.

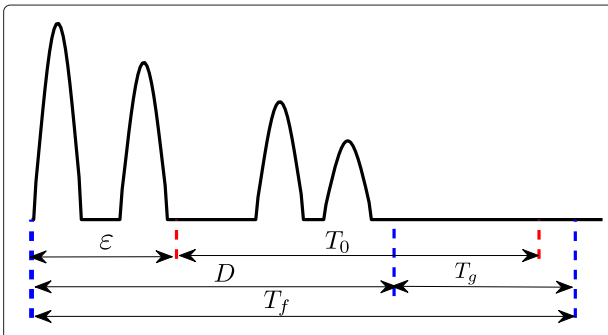

Figure 5 A GFSK frame structure in the presence of synchronization errors.

$\rho E_s, N_0^2 TW + 2N_0 \rho E_s$). And $Z_{j,1}$, $Z_{j,2}$, and $Z_{j,3}$ have the same pdfs $Z_{j,1} = Z_{j,2} = Z_{j,3} \sim N(N_0 TW, N_0^2 TW)$. Following the same method in Section 3, we achieve the SER in the presence of synchronization errors.

$$P_e = 1 - \left(1 - Q\left(\frac{\rho E_s}{\sqrt{2N_0^2 TW + 2N_0 \rho E_s}}\right)\right)^3 \quad (24)$$

And the equation for M-ary modulation is

$$P_e = 1 - \left(1 - Q\left(\frac{\rho E_s}{\sqrt{2N_0^2 TW + 2N_0 \rho E_s}}\right)\right)^{M-1} \quad (25)$$

where ρ denotes the ratio of the captured signal energy when synchronization error ε occurs. Due to the randomness of channel parameters, there is no direct equation to express ρ according to ε [4]. We can follow the method in [4] to achieve the value of ρ. The SER must be averaged over many channel realizations. In Section 6, the detailed method will be described. When $M = 2$, Equation 25 is reduced to

$$P_e = Q\left(\frac{\rho E_s}{\sqrt{2N_0^2 TW + 2N_0 \rho E_s}}\right) \quad (26)$$

It is the same as that in [4].

6 Numerical results, analysis and discussions

The SER equations for binary GFSK are proven validated in [4]. From the above analysis, we can know that the M-ary SER equation can be converted to the SER equation for binary modulation when the value of $M = 2$. So, the SER equations of the M-ary modulation are general equations which can be applied to any M-ary modulation including the binary modulation. In the following, we will compare the performance of binary and M-ary modulation using both the simulated and analytical SER curves. We use the SER equations to generate analytical SER curves directly. In this paper, we use 4-ary as an example to compare with binary modulation. We consider the pulses in Figure 1. The filter bandwidth is 1.66 Ghz.

Figures 6 and 7 show the SER performance comparisons of binary and 4-ary GFSK in multipath channels. The CM4 model [16] is used in SER calculation. Synchronization is perfect, and the maximum channel spread D is truncated to 80 ns. The frame length is designed using the method mentioned in Section 4, so IFI is avoided in SER calculation. In analytical SER calculation, we need to know the value of λ in Equations 21 and 23. Since there is no direct equation to calculate the captured energy respective to the integration interval, we follow the method in [4] to achieve the value of λ as follows. We use the MATLAB code in [16] to generate the realization of channel impulse response $h(t)$. And then we calculate the ratio of the captured energy in specific interval to the total energy of the channel realization to achieve the value of λ. Both the simulated and analytical SER is averaged over 100 channel realizations. We will compare the performance of these two modulations under different integration intervals. In Figure 6, when the integration interval T_0 is 80, 40, and 25 ns, the binary GFSK all achieves a 0.4-dB improvement at $SER = 10^{-5}$. The simulated and analytical SER curves all match well.

In Figures 8 and 9, the performances of binary GFSK and 4-ary GFSK are compared in the presence of synchronization errors. In SER calculation, the frame length is set to the maximum channel spread D. And the SER is achieved by using Equations 21 and 23 directly. Similarly, the value ρ in Equations 21 and 23 are achieved by using the similar method above. When synchronization errors are $\varepsilon = 0, 2$, and 4 ns, the binary GFSK all achieve a 0.4-dB improvement at $SER = 10^{-5}$. The simulated SER curves all match analytical SER curves well.

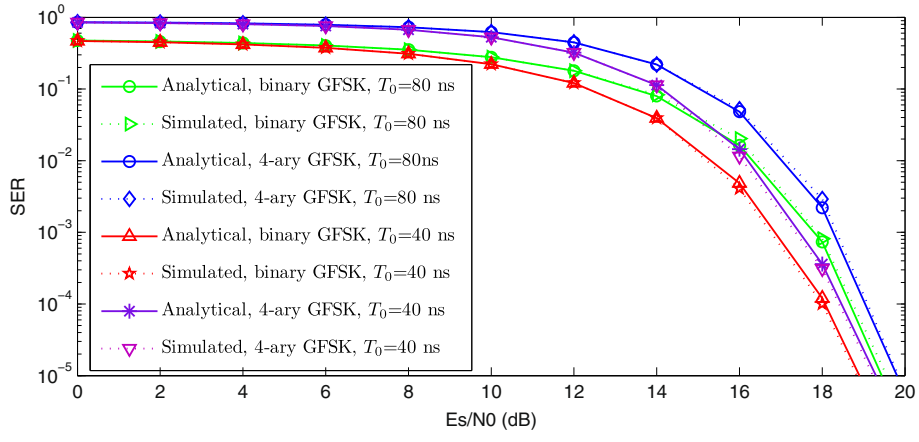

Figure 6 Comparisons of SER performances of binary and 4-ary GFSK in multipath channels. CM4 model, $D = 80$ ns, $T_0 = 80$ and 40 ns.

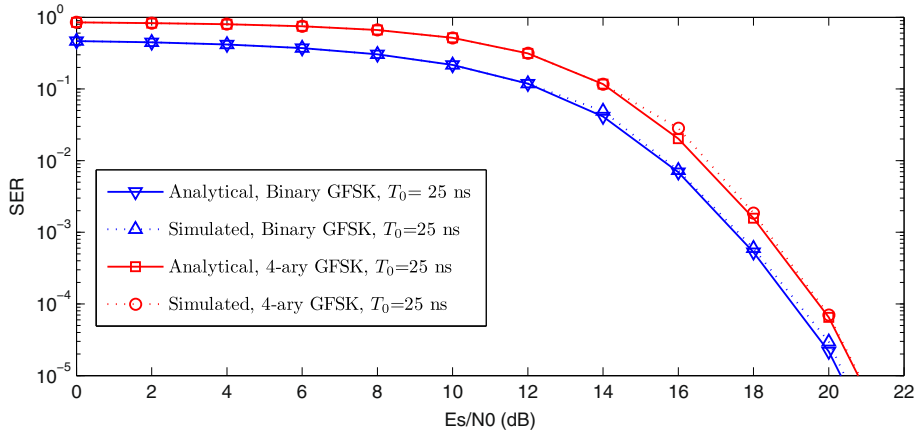

Figure 7 Comparisons of SER performances of binary and 4-ary GFSK in multipath channels. CM4 model, $D = 80$ ns, T_0= 25 ns.

From above numerical analysis, we can know that binary GSFK achieves a consistent 0.4-dB improvement under different integration intervals T_0 or synchronization errors. However, the 4-ary can deliver a speed that is twice that of the binary modulation. It is significant that the 0.4-dB loss of performance can achieve a double speed. There is always a trade-off between binary and M-ary modulations. The M-ary can deliver higher data rate but it causes performance loss. The designers should consider the actual applications to decide what kind of modulation to choose. If the speed is the primary requirement, the M-ary is a better option. If the performance is the most important condition to consider, binary is more suitable.

But if we use BER to compare the performance, the conclusion is different. When we look at Figure 1, because a symbol can be converted to any other three symbols with the same probability, any symbol error will lead to the $\frac{1}{2} * \frac{1}{3} + 1 * \frac{1}{3} + \frac{1}{2} * \frac{1}{3} = \frac{2}{3}$ bit error. And the relationship between E_b/N_0 and E_s/N_0 is $E_s/N_0 = \log_2 4 * E_b/N_0 = 2\frac{E_b}{N_0}$. We can convert Equation 22 into

$$P_b = \frac{2}{3}\left(1 - \left(1 - Q\left(\frac{\lambda 2E_b}{\sqrt{2N_0^2 TW + 2N_0\lambda 2E_b}}\right)\right)^3\right) \tag{27}$$

Figure 10 shows the simulated and analytical BER curves. The analytical BER curves are generated using Equation 27. When $T_0 = 80$ ns, the 4-ary achieves about 5.6-dB improvement at BER= 10^{-5}. When $T_0 = 40$ ns, the 4-ary achieves about 5.8-dB improvement at BER=

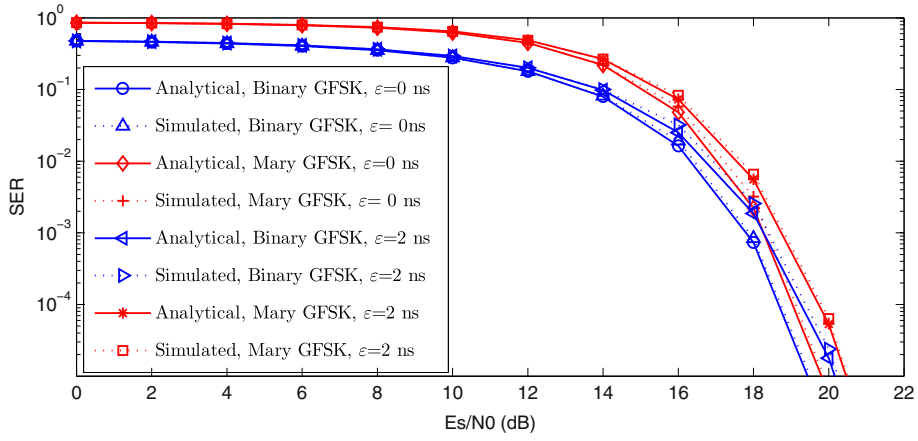

Figure 8 Comparisons of SER performances of binary and 4-ary GFSK in the presence of synchronization errors. CM4 model, $T_0 = D = 80$ ns, $\varepsilon = 0$ and 2 ns.

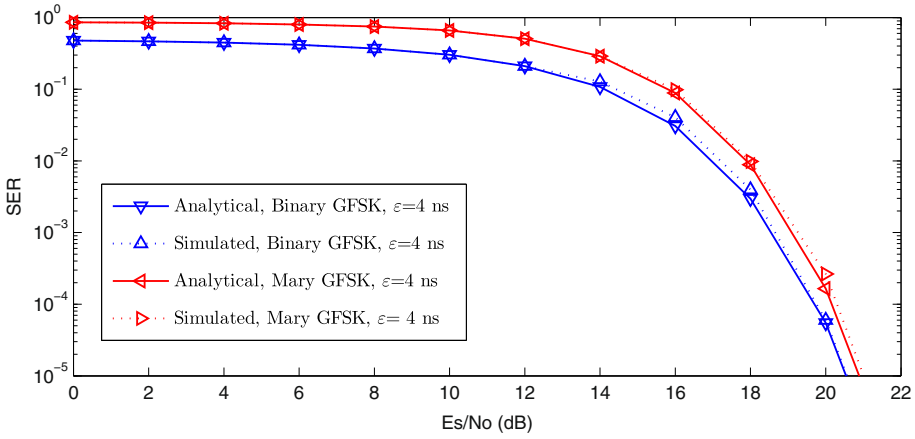

Figure 9 Comparisons of SER performances of binary and 4-ary GFSK in the presence of synchronization errors. CM4 model, $T_0 = D = 80$ ns, $\varepsilon = 4$ ns.

10^{-5}. Because in binary, a symbol error leads to an entire bit error. However, the 4-ary still can achieve some correct bits. Also, every bit in 4-ary convey less energy. So when we use BER to compare performance, 4-ary actually achieves better BER performance.

The implementation of high-order derivatives of the Gaussian pulse can be achieved by two approaches. The first one is the digital approach. The discreet points of waveforms are stored in the memory of application-specific integrated circuit (ASIC) or field programmable gate array (FPGA) chips. These points are sent to digital to analog converter (DAC), and then the DAC outputs the analog waveform of the pulse. This approach is straightforward and easy to achieve the waveform accurately. UWB pulses usually have large bandwidth, so it needs high sampling rate of the digital signal to recover the analog signal. The DAC needs to work in high clock rate. The burden of digital implementation is added on DAC. If we implement the pulse waveform by analog approach, it will not need high-speed DAC. The system will send the control signal to activate the corresponding pulse generator respective to the specific data. The design of analog pulse generator is not so straightforward as the digital approach. There are many analog research achievements on UWB pulse generators. In [17], a 7th-order pulse generator is proposed. In [18], the pulse generator arrives to the 13th order. The pulse generator in [19] can generate the pulse with a center frequency at 34 GHz. The higher the order of the pulse is, the higher the center frequency is. The pulse generator in [19] has the ability to generate pulse with higher center frequency than the range of 3.1 to 10.6 GHz set by FCC. These research achievements have already provided feasible solutions for analog implementation of high-order derivative of the Gaussian pulse. We

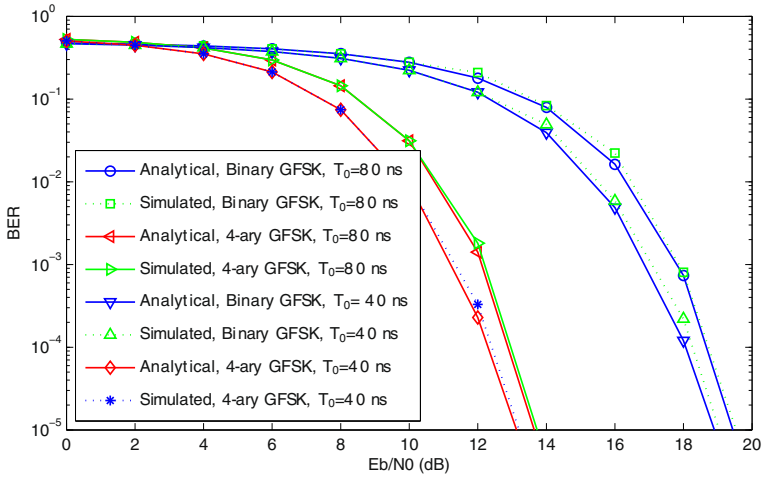

Figure 10 Comparisons of BER performances of binary and 4-ary GFSK in multipath channels. CM4 model, $D = 80$ ns, $T_0 = 80$ and 40 ns.

do not provide any specific circuit design in this paper and it is left for the hardware engineers or researchers.

7 Conclusion

The M-ary energy detection GFSK UWB system is proposed. The system performance is analyzed in AWGN channels, multiple channels, and in the presence of synchronization errors. The M-ary system can achieve higher data rate than binary system. However, it causes the performance loss.

Competing interests
The authors declare that they have no competing interests.

Received: 9 December 2013 Accepted: 25 April 2014
Published: 29 May 2014

References

1. N Zhang, T Zhang, Q Zhang, A study on performance of an IR-UWB receiver based on energy detection, in *Proceedings of the IEEE International Conference on WiCOM* (Dalian, China, September 2008), pp. 19–21
2. D Mu, Z Qiu, Weighted non-coherent energy detection receiver for UWB OOK systems, in *Proceedings of the 9th IEEE International Conference Signal Processing* (Beijing, China, October 2008), pp. 26–29
3. S Dubouloz, B Denis, S Rivaz, L Ouvry, Performance analysis of LDR UWB non-coherent receivers in multipath environments, in *Proceedings of the IEEE International Conference on Ultra-Wideband* (Zurich, Switzerland, 5–8 September 2005)
4. S Cui, F Xiong, UWB system based on energy detection of derivatives of the Gaussian pulse. Eurasip J. Wireless Commun. Netw. **2011**, 206 (2011)
5. C Mitchell, R Kohno, High data rate transmissions using orthogonal modified hermite pulses in UWB communications, in *Proceedings of the 10th IEEE ICT* (Papeete, Tahiti (French Polynesia), 23 Feb–1 Mar 2003)
6. Y Kim, B Jang, C Shin, B Womack, Orthonormal pulses for high data rate communications in indoor UWB systems. IEEE Commun. Lett. **9**(5), 405–407 (2005)
7. F Ramirez-Mireles, Analysis of M-ary UWB FSK detected using two passband filters considering antenna and multipath effects, in *IEEE MILCOM* (Orlando, FL, 29 Oct–1 Nov 2012)
8. MZ Win, RA Scholtz, Impulse radio: how it works. IEEE Commun. Lett. **2**(2), 36–38 (1998)
9. X Cheng, YL Guan, Mitigation of cross-modulation interference in UWB energy detector receiver. IEEE Commun. Lett. **13**(6), 375–377 (2009)
10. H Celebi, H Arslan, Cross-modulation interference and mitigation technique for ultrawideband PPM signaling. IEEE Trans. Veh. Tech. **57**(2), 847–858 (2008)
11. F Wang, Z Tian, B Sadler, Weighted energy detection for non-coherent ultra-wideband receiver design. IEEE Trans. Wireless Commun. **10**(2), 710–720 (2011)
12. J Wu, H Xiang, Z Tian, Weighted non-coherent receiver for UWB PPM signal. IEEE Commun. letters. **10**(9), 655–657 (2006)
13. J Almodovar-Faria, J McNair, D Wentzloff, Optimal receiver bandwidth for energy-detection PPM UWB systems, in *Proceedings of the IEEE WCNC* (Cancun, Mexico, 28–31 March 2011)
14. K Katsu, D Anzai, J Wang, Performance evaluation on correlation detection and energy detection for ultra wideband-impulse radio communication with multi-pulse position modulation scheme in implant body area networks. IET Commun. **7**(13), 1430–1436 (2013)
15. RF Mills, GE Prescott, A comparison of various radiometer detection models. IEEE Trans. Aero. Elec. Sys. **32**(1), 467–473 (1996)
16. AF Molisch, K Balakrishnan, D Cassioli, C Chong, S Emami, A Fort, J Karedal, J Kunisch, H Schantz, U Schuster, K Siwiak, IEEE 802.15.4a channel model-final report. (IEEE Website), http://www.ieee802.org/15/pub/04/15-04-0662-02-004a-channel-model-final-report-r1.pdf. Accessed June 2011
17. T Phan, V Krizhanovskii, S-K Han, S-G Lee, H-s Oh, N-S Kim, 4.7pJ/pulse 7th derivative Gaussian pulse generator for impulse radio UWB, in *IEEE Int. Sym. Cir. Sys* (New Orleans, LA, 27–30 May 2007)
18. D Kim, G Bang, C Park, Design and characteristics of high order derivative Gaussian pulse generator for DS-UWB, *IEEE Asia-Pacific Microwave Conference* (Yokohama, Japan, 12–15 Dec 2006)
19. A Zadok, X Wu, J Sendowski, A Yariv, AE Willner, Reconfigurable generation of high-order ultra-wideband waveforms using edge detection. J. Lightw. Tech. **28**(16), 2207–2212

doi:10.1186/1687-1499-2014-87
Cite this article as: Cui and Xiong: **M-ary energy detection of a Gaussian FSK UWB system.** *EURASIP Journal on Wireless Communications and Networking* 2014 **2014**:87.